J Mater Sci (2021) 56:10834–10846

Chemical routes to materials

Synthesis and characterization of WS_2/SiO_2 microfibers

Vojtech Kundrat[1], Rita Rosentsveig[2], Olga Brontvein[3], Reshef Tenne[2,*], and Jiri Pinkas[1,4,*]

[1] Department of Chemistry, Masaryk University, Kotlarska 2, 61137 Brno, Czech Republic
[2] Department of Materials and Interfaces, Weizmann Institute of Science, 76100 Rehovot, Israel
[3] Department of Chemical Research Support, Weizmann Institute of Science, 7610001 Rehovot, Israel
[4] CEITEC MU, Masaryk University, Kamenice 5, 62500 Brno, Czech Republic

Received: 10 November 2020
Accepted: 2 March 2021
Published online: 17 March 2021

ABSTRACT

Tungsten disulfide polycrystalline microfibers were successfully synthesized by a process involving electrospinning, calcination, and sulfidation steps. We used an aqueous solution of silicotungstic acid ($H_4SiW_{12}O_{40}$) and polyvinyl alcohol as precursors for the synthesis of composite fibers by the needle-less electrospinning technique. The obtained green composite fibers (av. diam. 460 nm) were converted by calcination in air to tungsten oxide WO_3 fibers with traces of SiO_2 and a smaller diameter (av. diam. 335 nm). The heat treatment of the WO_3 fibers under flowing $H_2/H_2S/N_2$ stream led to conversion to tungsten disulfide WS_2 with retention of the fibrous morphology (av. diam. 196 nm). Characterization of the intermediate and final fibers was performed by the XRD, SEM, TEM, HAADF STEM EDS, elemental analyses ICP-OES, and IR spectroscopy methods.

GRAPHICAL ABSTRACT

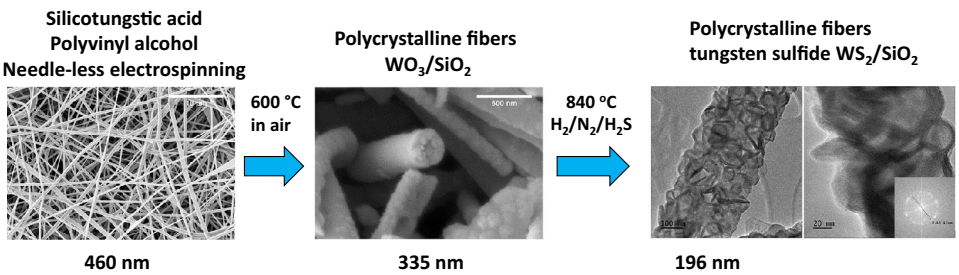

Handling Editor: N. Ravishankar.

Address correspondence to E-mail: reshef.tenne@weizmann.ac.il; jpinkas@chemi.muni.cz

https://doi.org/10.1007/s10853-021-05979-y

Introduction

Electrospinning is a well-established method for the preparation of many types of materials with general nanofibrous morphologies [1]. An electrode, in the form of a syringe needle or free surface of a polymer solution, is electrically charged and a Taylor cone is formed from the droplet or surface. A jet of the evaporating solution is drawn toward a grounded or negatively charged counter electrode which serves simultaneously as a collector of solidified polymer fibers. This technique, closely resembling electrospraying, is exploited for obtaining various fibrous morphologies: micro- and submicron fibers, nanofibers, hollow fibers, Janus-type fibers, porous structures, interconnected fibrous membranes, branched fibers and many other shapes [1–3]. The process is controllable by many variables, where the composition of the spinning solution is a dominant factor next to the applied voltage, electrode distance, feed rate, and several others [3]. Electrostatic spinning is used for the preparation of purely organic fibers where almost all regular and even modified polymers were successfully electrospun to form ultrafine or at least submicrometric fibers. However, not only these classical systems could be processed, and nowadays, we can witness intensive research on the fabrication of inorganic, purely ceramic, and mixed composite fibers by this technique [4, 5]. Many oxides, carbides, nitrides, and multimetallic compounds, such as perovskites and spinels, have been reported [1]. Inorganic nanofibers could be used in many already existing applications including energy storage, battery cathodes or anodes, catalysts, fillers in composite materials, gas sensors, and as precursors of fine ceramics [6]. Following the electrospinning process, green composites of inorganic precursors and organic polymers are formed. To obtain pure oxide ceramic fibers, it is necessary to remove the organic polymer matrix, in most cases, via high temperature burn up in an air atmosphere. Additional variables are thus involved, such as maximum firing temperature, time and rate of heating, and the used atmosphere. The ambient gas has a special importance during the annealing treatment after removal of the polymer in air atmosphere. By using various gaseous mixtures or pure gasses, it is possible to obtain diverse inorganic compounds in the form of ultrafine fibers. For example, reducing atmosphere could lead in some cases to purely metallic polycrystalline fibers or utilization of, e.g., ammonia, methane, and hydrogen sulfide, produces nitrides, carbides, or sulfides, respectively [7–9]. An advantage of the described method is the facile scale-up of micro- and nanofiber fabrication process via needle-less electrospinning from the solution surface, which potentially allows building an industrial-level production line with continuous operation [10–12].

Electrospinning of tungsten-containing fibers has to be based on a soluble inorganic precursor of this element. Simultaneously, it has to be transformed by after-spinning processes to a form, which is suitable for subsequent reactions without impurity elements, which could cause the formation of undesirable phases. In practical terms that dictates usage of water-soluble ammonium tungstates, tungstic acid, or other precursors forming tungsten trioxide by heat treatment in an oxygen atmosphere. Selection of the right precursor could be a challenging task due to the limited solubility of some precursors, such as the already mentioned tungstic acid or ammonium paratungstate. Much more soluble ammonium metatungstate, however, suffers from a high cost, which could be prohibitive for production on a multigram scale. Sodium tungstate, which is easily soluble in aqueous solvents, however, cannot be used due to the presence of unwanted sodium cations, which will remain embedded in the material even after a high-temperature treatment. Finding a proper precursor for industrial scale-up from laboratory conditions, therefore, is not straight forward.

Silicotungstic acid, $H_4SiW_{12}O_{40}$, is polyoxometalate acid consisting of 12 tungsten atoms and one silicon atom all compensated by oxides and four hydrogens forming a Keggin-type structure where silicon resides in the central tetrahedral cavity of a W_{12} cage. This compound is mostly applied as a catalyst for a broad spectrum of reactions, even on an industrial scale. Production of ethyl acetate and acetic acid from ethylene via catalysis by silicotungstic acid was commercialized by Showa Denko [13]. Also, a significant application could be found as an additive to fuel cell membranes enhancing proton conductivity [14]. Silicotungstic acid is highly soluble in aqueous systems and we used it here as an inorganic precursor for the electrospinning process.

Tungsten disulfide WS_2 is a layered (2D) semiconducting material with many promising applications in electronics, optoelectronics, catalysis, gas

sensors, lubricants, biomedicine, and energy storage [15–21]. It has been prepared in the form of nanoplates, thin films, nanotubes, fullerene-like nanoparticles [22–24], quantum dots [25], rods, and fibers [26].

In the present work, the silicotungstic acid/polyvinyl alcohol (PVA) solution was electrospun via a scaled-up needle-less electrospinning procedure to green composite fibers that by calcination in air formed submicron polycrystalline fibers consisting of WO_3/SiO_2. Subsequently, H_2S treatment of the annealed tungsten oxide fibers was undertaken, according to a procedure which was extensively used for sulfidation of pure WO_{3-x} nanoparticles [27], providing tungsten disulfide WS_2 microfibers.

Experimental

General

Polyvinyl alcohol (PVA, Mowiol 18–88, M = 130 000 g mol^{-1}) and silicotungstic acid hydrate (purum) were obtained from Sigma-Aldrich and used as received. Deionized water was used as a solvent. For electrospinning, a Nanospider NS LAB500S (Elmarco, Czech Republic) system was used equipped with a cylindrical electrode with microblades for localization of electrical charge and solution droplets. [10, 28] (Fig. 1).

The electrospinning process was performed under an ambient atmosphere in an air-conditioned room. The details of the electrospinning parameters are provided below. The prepared solutions were characterized before electrospinning by conductometry, viscosimetry, and surface tension measurements.

Preparation of electrospinning solution

PVA (150 g) was dissolved in deionized water (1150 g) by stirring and heating for several hours providing a 11.5 wt% solution. Silicotungstic acid hydrate (120 g) was dissolved in deionized water (200 g). Both solutions were combined at ambient temperature and homogenized by intensive stirring for several hours. A clear colorless viscous solution was formed and further characterized with respect to its physical properties (Table 1). The final polymer and tungsten precursor contents in the prepared solution were approx. 9.3 and 7.4 wt%, respectively.

Needle-less electrospinning

The prepared solution (approx. 800 cm^3) was transferred to the electrode vessel with a partially submerged electrode. A grounded counter electrode in the form of a stretched wire was covered with a large sheet of aluminum foil (approx. 0.8 × 0.4 m), and the electrode distance was set to 17.0 cm. The speed of the rotating electrode was set to 30 rpm. The applied voltage was set to 50 kV. The process was running for 4 h when half of the used solution was depleted, and the aluminum collector was covered by a thick layer of nonwoven felt of a green composite of PVA and silicotungstic acid. Electrospinning was interrupted due to a noticeable increase in viscosity of the solution. The increased viscosity was most probably caused by an increased rate of solvent evaporation from the relatively high surface area of the electrode and the solution. The solvent evaporation was exacerbated by ventilation of the chamber. The prepared fibrous material was peeled off, analyzed by SEM and TGA/DSC and used in further process.

Calcination and high-temperature treatment

Collected layers of electrospun fibers were treated in a muffle oven at 600 °C, which was set according to the TGA/DSC measurement. The oven was programmed to achieve the maximum temperature in 4 h followed by another 4 h at the constant temperature and finally spontaneous cool down to ambient temperature. After this heat treatment, the material was collected and analyzed.

High-temperature reaction with H_2S

The high-temperature sulfidation was carried out in a reducing atmosphere. The conditions of the process were similar to those used for the synthesis of other sulfide nanostructures [27].

The powder was placed into a quartz boat and then inserted into a quartz reactor. The reactor was purged continuously with N_2 in order to prevent traces of O_2 and moisture that would otherwise interfere with the course of the reaction. Then, the reaction gases—forming gas (H_2/N_2 at a ratio of 10/90) and H_2S—were added to the flow. Following this step, the reactor was inserted into a horizontal furnace, which was preheated to 840 °C and maintained at this temperature for 2 h. At this point, the boat was

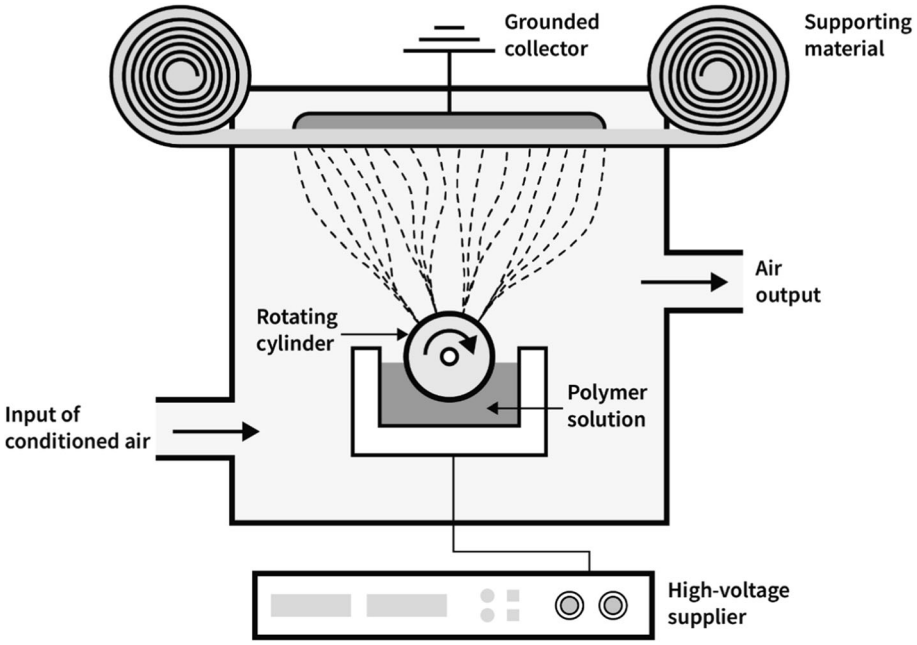

Figure 1 Submerged electrode equipped with microblades in Nanospider NS LAB500S [28].

Table 1 Properties of the electrospinning solution

Dynamic viscosity [mPa s] (21.6 °C)	258
Conductivity [mS cm^{-1}] (21.7 °C)	6.8
Surface tension [mN m^{-1}] (21.6 °C)	61.7 ± 0.3

moved out of the oven and left to cool spontaneously to room temperature.

During this entire series of steps, the reactor was purged with a continuous flow of reaction gases. Several experiments were run with various reaction conditions in order to study their possible influence on the result of the sulfidation process. The total flow rate was about 130–150 cm^3 min^{-1}. Composition of the gas flow was slightly varied between 5 and 10 cm^3 min^{-1} H_2, 7–10 cm^3 min^{-1} H_2S, and the rest was nitrogen carrier gas. The precursor powder was either placed directly into the quartz boat or into prefilled quartz crucibles, which were then placed in the boat.

Characterization of the solutions and powders

Thermogravimetric analysis

Thermogravimetric analysis and differential scanning calorimetry (TG/DSC) were performed using a Netzsch Jupiter STA 449 instrument with a heating rate of 10 K min^{-1} and a maximum temperature of 1000 °C.

Electrical conductivity, viscosity and surface tension of the solution

The electrical conductivity of the solutions was measured with a Cond51 conductometer (XS Instruments). Viscosity measurement was performed on an Alpha Fungilab rotational viscosimeter. Surface tension was determined by a Sigma 700 tensiometer equipped with a Wilhelmy probe.

Elemental analysis

Samples for elemental analysis were mineralized by a heat-induced reaction between excess sodium peroxide, glycerine, and the analyzed material itself followed by quantitative dissolution in deionized water of known volume. A typical procedure was as follows: a precise amount of a material (e.g., 0.2012 g) was mixed with two droplets of glycerin in small pressure reactor and covered with sodium peroxide (approx. 3 g). The reactor was tightly sealed and heated with a burner until the slight snap-like sound was induced. After cooldown, the content of the reactor was quantitatively transferred to an analytical flask and filled with deionized water. The prepared solution was analyzed by the inductively coupled plasma method (ICP-OES) using a spectrometer

iCAP 6500 Duo (Thermo, generator 27.12 MHz, amplitude 1.15 kW, plasma gas flow 12 dm^3 min^{-1}) emission lines 224.9 and 207.9 nm for W and 212.4 and 251.6 nm for Si.

IR spectroscopy

Infrared spectra were obtained on a Bruker Tensor 27 FTIR spectrometer with a Bruker Alpha-Platinum ATR system.

Powder X-ray diffraction

Powder X-ray diffraction (XRD) measurements were performed with a GNR Europe 600 diffractometer with a Co ($\lambda_{K\alpha}$ = 1.79030 Å) lamp and using a TTRAX III (Rigaku, Tokyo, Japan) θ–θ diffractometer. This set-up was equipped with a rotating copper anode X-ray tube operating at 50 kV/200 mA. A scintillation detector aligned at the diffracted beam was used after a bent Graphite monochromator. The samples were scanned in specular diffraction mode ($\theta/2\theta$ scans) from 10 to 80 degrees (2θ) with a step size of 0.025 degrees and a scan rate of 0.5 degrees per minute. Phase identification and quantitative analysis were performed using the Jade 2010 software (MDI) and PDF-4 + (2016) database.

Electron microscopy

The nanofibrous materials were characterized by scanning electron microscopy (SEM) using model Versa 3D (FEI/Thermo Fischer Scientific, Czech Republic) and Zeiss Sigma 500 microscopes. Transmission electron microscopy (TEM) characterizations were performed on an FEI Tecnai G2 instrument at 200 kV equipped with a 4 k CCD camera FEI Eagle. The samples for the TEM measurements were dispersed in methanol and 4 μL of the suspension. The suspension was dripped on a Quantifoil copper grid and allowed to dry by evaporation at ambient temperature.

The TEM analysis and HAADF STEM EDS measurements of WS_2 fibers were performed with a Titan Themis Z at 200 kV, equipped with two Rose-Haider double-hexapole aberration correctors (probe and image), a Super-X large solid angle X-ray detector for EDS and a OneView high-speed CMOS camera for wide-field TEM imaging. The sample for the TEM measurements was dispersed in ethanol, then dripped on a copper grid and dried at ambient conditions.

SEM micrographs were analyzed by the ImageJ software for fiber diameter and size distribution.

Results and discussion

The composition of the electrospun solution was optimized for the maximal simplicity of the mixture. Silicotungstic acid was found as a precursor widely used in industry and satisfying demands for high water solubility and a high content of tungsten. Polyvinyl alcohol (PVA) was found to be suitable for electrospinning, being an inexpensive, easily accessible, and water-soluble material. It is available in a range of average chain lengths, different degrees of hydrolysis, and polydispersity [29, 30]. Mowiol 18–88 was chosen from all variants as the most common polymer from PVA families, which is also well soluble in comparison with fully hydrolyzed compounds [31].

Conductometric characterization of the starting solution provided an elevated value of 6.8 mS cm^{-1} in comparison with 1 mS cm^{-1} for the PVA solution. This is due to the dissociation of added silicotungstic acid. The surface tension (61.7 mN m^{-1}) was lower than the tabulated value for water 72.86 mN m^{-1} [32] at approximately the same temperature. In general, lower surface tension means lower electrical force needed to initiate the electrospinning process because the Taylor cone is in a stable equilibrium between the electrical force field and surface tension [1]. Decrease in the surface tension also helps to prevent the formation of beaded structures on the fibers [1].

The electrospinning was performed via multi-jet spinning from free surface enhanced by blades on the electrode. The rotation speed of the electrode was set to ensure that the electrode is wetted by the solution during the entire cyclic movement. The transferred mass was collected on an aluminum foil electrode, where at first a thin layer of a white fabric formed, which turned to a thick 3D web of white material at the end of the electrospinning process. The fibrous mat was peeled off, collected, and analyzed by scanning electron microscopy (SEM) and thermal analysis (TGA/DSC).

The SEM measurements provided insight into the morphology of the prepared mats consisting of submicron fibers with a broad distribution and with an

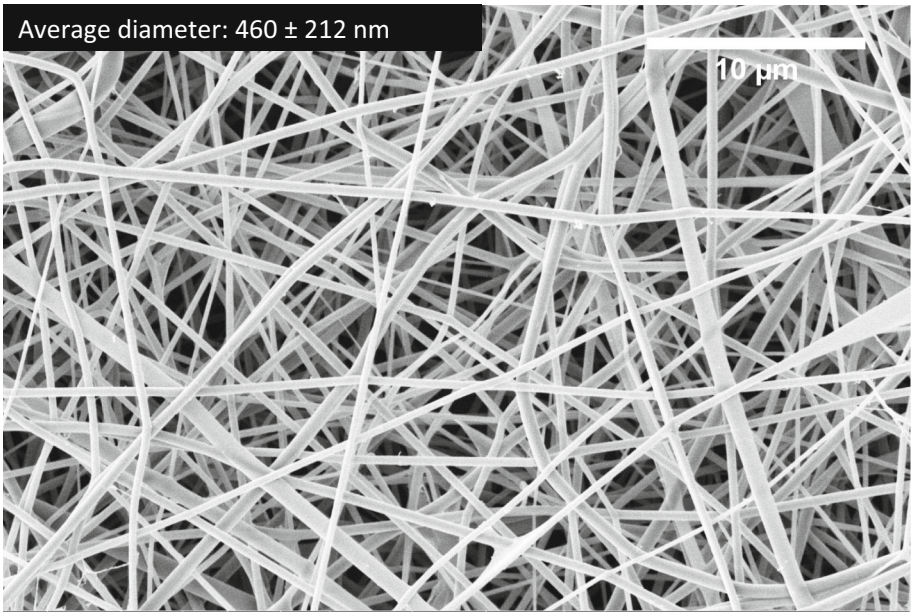

Figure 2 SEM image of a green composite fibers of PVA and silicotungstic acid.

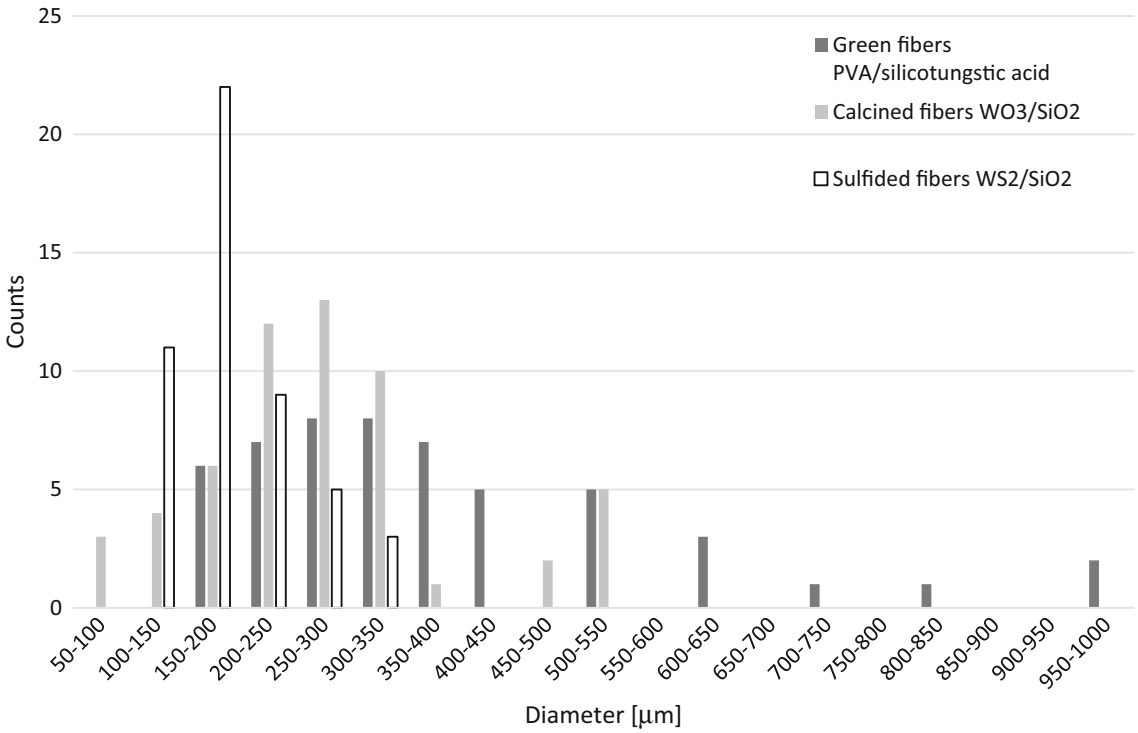

Figure 3 Distribution of the fiber thickness of a green composite of PVA and silicotungstic acid (black), its calcined product $(WO_3)_{12}$/SiO_2 (gray), and the sulfided WS_2 fibers (white).

average thickness of 460 nm (Fig. 2). These results correlate well with literature values of PVA electrospun fibers [33], which lay in a submicron range and typical hundred-nanometer thickness. It is possible to observe a few flat ribbon-like fibers, which are typical for PVA solutions with a relatively high concentration and viscosity [1]. Thinner fibers are present with a diameter around 200–300 nm (Fig. 3—black).

TG/DSC analysis (Fig. 4) was used to find a proper calcination temperature. Heating the sample causes steadily decreasing mass, followed by exothermic

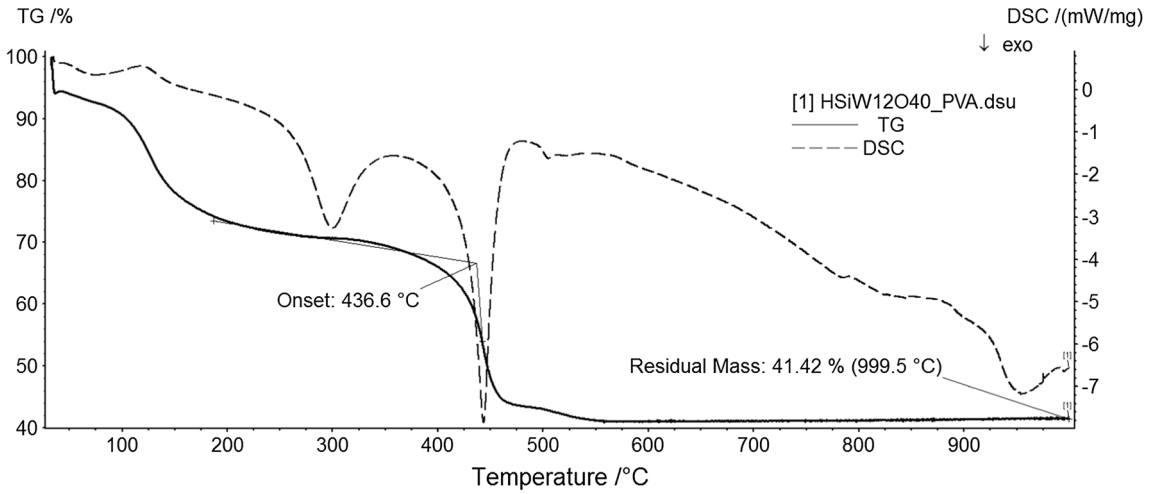

Figure 4 TG/DSC traces measured in air of a green composite PVA and silicotungstic acid.

Table 2 Elemental analysis of calcined $(WO_3)_{12}/SiO_2$ fibers by ICP-OES

	w	σ	$w_{Nominal}$	w_W/w_{Si}	w_w/w_{Si}
	[%m/m]	[%m/m]	[%m/m]	Exp	Nominal
Si	0.973	0.010	0.988	76.98	78.55
W	74.9	1.0	77.6		

burnout of the polymer matrix with an onset temperature of 437 °C. After exothermic removal of most of the organic material, a smaller decrease in mass is observed; however, the mass remains stable above 550 °C. Based on the results of the TG/DSC measurement, we have selected the calcination temperature of 600 °C.

The green composite fiber mat was transferred into an alumina crucible and calcined under air by steadily increasing the temperature up to 600 °C within 4 h followed by another 4 h at this temperature. Calcination was concluded by free cooldown to an ambient temperature. The white fibers were transformed into yellow-greenish brittle flakes, which were further analyzed by SEM, TEM, XRD, ICP-OES, and IR spectroscopy methods.

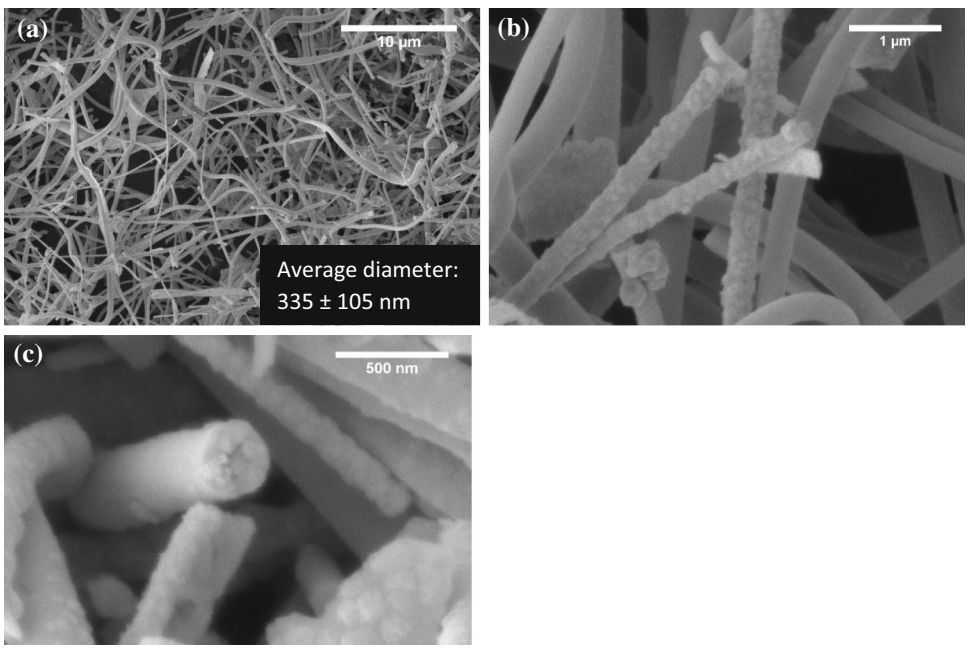

Figure 5 SEM images of the calcined composite of PVA and silicotungstic acid. $(WO_3)_{12}/SiO_2$ fibers with even surface (**a**), fibers with non-uniform surfaces (**b**), high-magnification of the annealed oxide fibers (**c**).

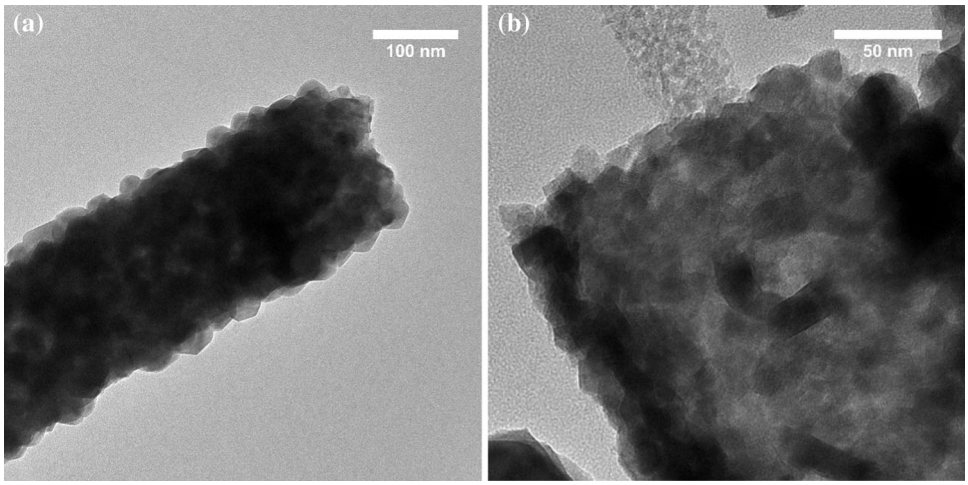

Figure 6 TEM image of a calcined $(WO_3)_{12}/SiO_2$ fiber (**a**) and its detailed structure (**b**).

Table 3 Summary of FFT and XRD analysis data on WO_3 fibers

Spacing from FFT [nm/c]	*d* [Å]	Miller indices
0.26–0.27	2.6–2.7	202, 220
0.31	3.1	112
0.365	3.65	200
0.38	3.8	002, 020

Quantitative elemental analysis of mineralized samples of calcined fibers by the ICP-OES method revealed concentrations of tungsten and silicon close to the theoretical values for a mixture of oxides $(WO_3)_{12}/SiO_2$ resulting from thermal decomposition of $H_4SiW_{12}O_{40}$ (Table 2). This stoichiometric ratio implies a complete conversion of the silicotungstic acid precursor to the bulk fibers.

From the electron microscopy analysis, it is evident that the calcined material has a polycrystalline fibrous structure in the submicron range of fiber thickness. The SEM images of the calcined material (Fig. 5a) show entangled array of fibers with a cylindrical cross section and fairly even surface morphology. On the other hand, Fig. 5b shows that in some other areas, many fibers exhibit rough surfaces with oxide bulges, indicating secondary precipitation of the oxide upon cooling of the specimen. Individual fibers are composed of crystallites (Fig. 5c). An average diameter has been measured with the ImageJ software from 50 individual fibers. Analysis of the size histogram (Fig. 3—gray) revealed an average diameter of 335 nm with a relatively broad distribution.

In comparison with the green fibers, it is observed that the average diameter of $(WO_3)_{12}/SiO_2$ fibers, i.e., following calcination, decreased; however, when the standard deviation is taken into account, both samples are comparable even from the mean thickness point of view. The slight shrinking of the fiber thickness can be attributed to the removal of the organic matrix from the green composite during calcination. Comparing both histograms provides identical size distribution; however, in the calcined sample also fibers with very thin diameters of 100 nm are present. It is also remarkable that the calcined fibers are curled compared to the green fibers, which are quite straight. Furthermore, many annealed fibers are broken into short sections, indicating lower fracture toughness of the annealed fibers.

Detailed SEM measurements, together with TEM analysis (Fig. 6), describe the $(WO_3)_{12}/SiO_2$ fibers as agglomerates of nanoparticles with crystalline structure analyzable by FFT to provide a complementary measurement to the XRD method. The result of this analysis is shown in the Supplementary material (Fig. 1S). The spacing of the crystal planes correlates well with the Miller indices from the XRD diffractogram. Diffractogram with corresponding Miller indices and *x*-axis in Å is shown in the Supplementary material (Fig. 2S). The results of the FFT analysis and XRD are summarized in Table 3. Determination of the fine structure of thick fibers by TEM analysis was challenging (Fig. 6a). However, analysis of thinner fibers (less than 150 nm) permitted observing the crystal planes (Fig. 6b). XRD measurement (Fig. 7) provided diffractions of the WO_3 phase according to the COD database card [COD-1528915].

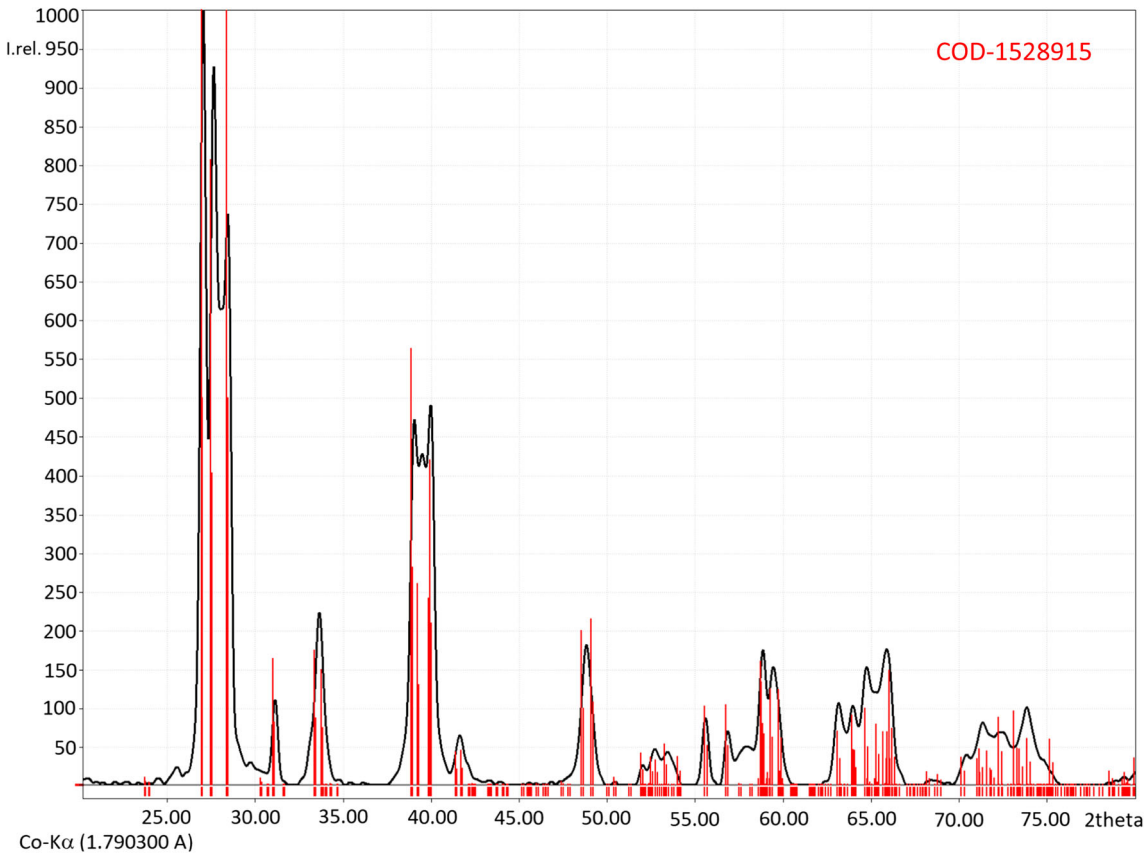

Figure 7 XRD diffractogram of the calcined $(WO_3)_{12}/SiO_2$ fibers. Red vertical lines represent the diffraction pattern of WO_3 (COD-1528915).

Silica remains amorphous under these synthetic conditions and presents no diffractions. Several planes in the crystal lattice of WO_3 were recognized (Table 3), mainly (200), (020), (002) as the Miller indices of the corresponding planes.

The prepared material was analyzed also by infrared spectroscopy. The IR spectra are shown in the Supplementary material (Fig. 3S). The bands observed in the infrared spectra are consistent with the presence of W–O–W (400–1000 cm^{-1}) and Si–O–Si (1000–1200 cm^{-1}) deformation vibrations [34].

A high-temperature sulfidation reaction was carried out on the fibers in forming gas (H_2/N_2) and H_2S with the aim of converting WO_3 to WS_2 while maintaining the fiber morphology. The reaction converted the green-yellowish fibers into a black powder. The XRD diffractogram (Fig. 8) of the sulfided fibers shows that all the peaks can be indexed to the 2H-WS_2 phase COD-9012191. This finding suggests that the silica islands in the fiber have not been affected and remain amorphous following this high-temperature (840 °C) reaction.

The SEM analysis (Fig. 9) of the sulfided samples revealed the average diameter of the fibers was 196 ± 54 nm. The images indicate that, in analogy to the oxide fibers, two kinds of morphologies are present: fibers with rough surfaces (a) and even surfaces (b). In the fibers with rough surfaces, the flakes are arranged as nanoflowers [35], which seem to emanate from a single bulge on the oxide fiber surface. In the fibers with even surfaces, the *a-b* plane of the flakes is presumably parallel to the fiber surface, i.e., their *c*-axis is perpendicular to the growth axis of the fiber. High-resolution TEM of a "rough" fiber shows clearly that the nanoflakes stand out of the fiber surface (< hk0 > direction perpendicular to the fiber surface).

From the TEM images (Fig. 10), it can be seen that the fibers are made of small layered flakes arranged randomly with respect to the fiber axis. The measured interlayer spacing is 6.2 Å, which corresponds well to the WS_2 interlayer distance.

From the HAADF STEM EDS measurements (Fig. 11) and quantitative measurements of selected

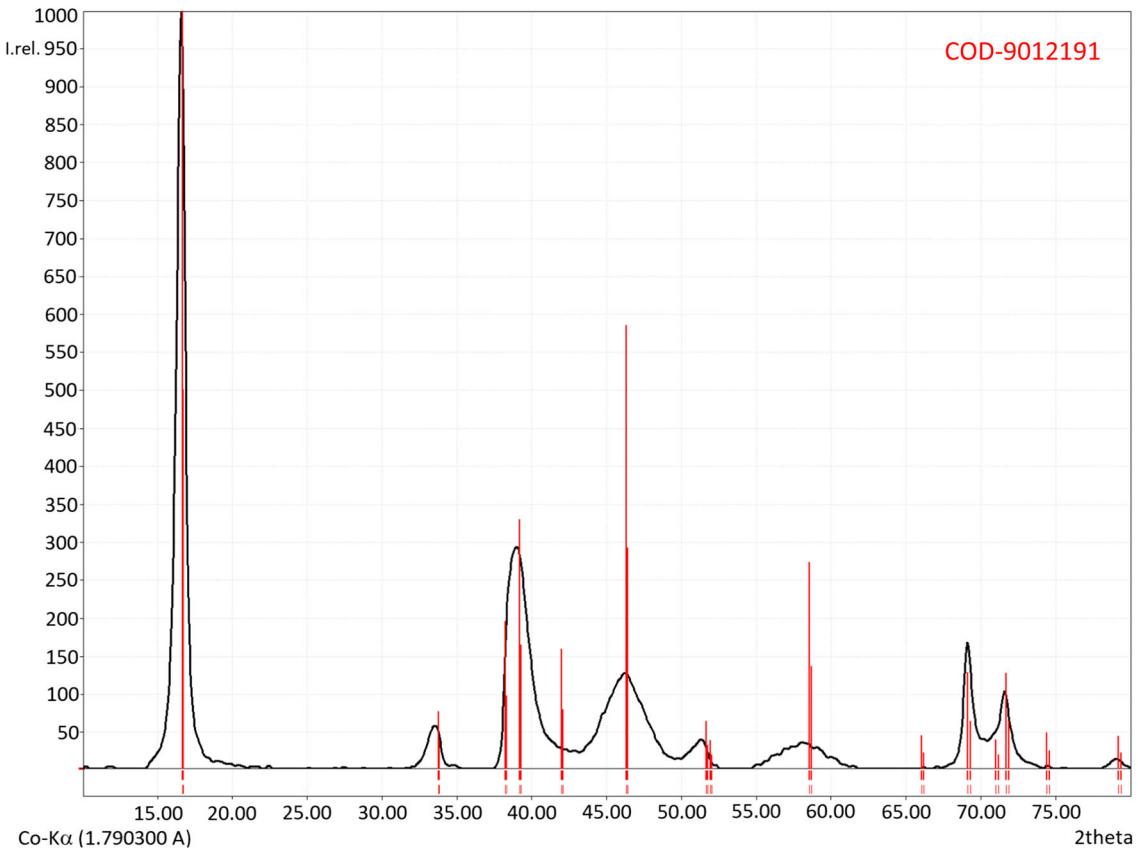

Figure 8 XRD diffractogram of WS_2/SiO_2 nanofibrous composite with red vertical lines representing the diffraction of 2H-WS_2 (COD-9012191).

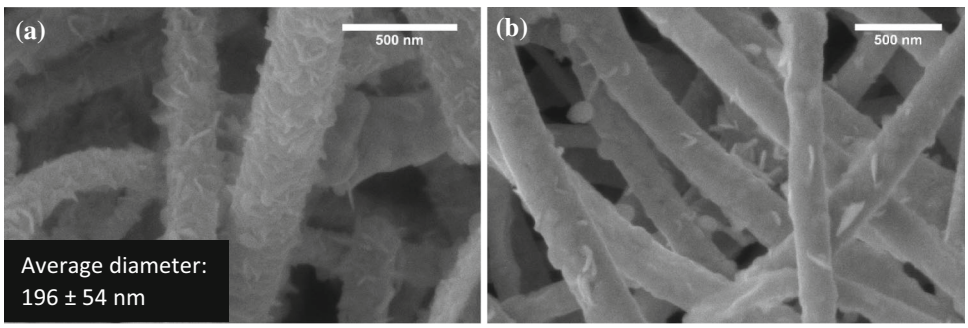

Figure 9 SEM analysis of the sulfided fibers with rough surfaces (**a**) and even surfaces (**b**).

areas (Table 4), it can be concluded that the fibers are composed of tungsten and sulfur with a 1:2 atomic ratio (WS_2) interspersed by SiO_2 islands. The analysis indicates that the amorphous silica serves as a binder for the WS_2 flakes in the fiber. Such a configuration imparts mechanical robustness for the WS_2 flakes, which are well-separated from each other in the fiber. Therefore, the present fiber morphology could serve as a highly reactive catalyst for different reactions or sensor for different gases.

Conclusion

We prepared tungsten disulfide WS_2 fibers by a three-step process. In the first step, we used the needle-less electrospinning technique with an aqueous solution of silicotungstic acid ($H_4SiW_{12}O_{40}$) and polyvinyl alcohol (PVA) as precursors for the preparation of composite green fibers. The obtained fibers (av. diam. 460 nm) were converted in the second step by calcination in air into tungsten

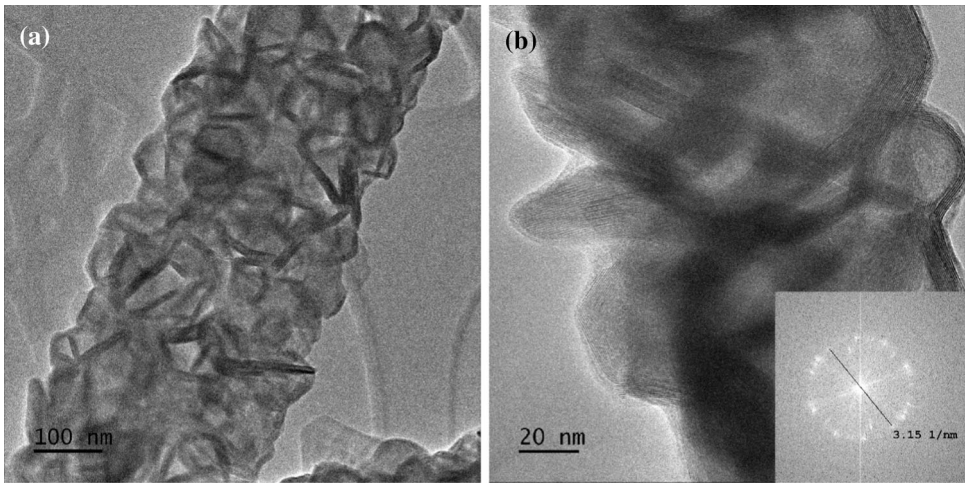

Figure 10 TEM image of WS_2 fibers (**a**), a high-resolution TEM image of WS_2 fibers, inset FFT of image (**b**).

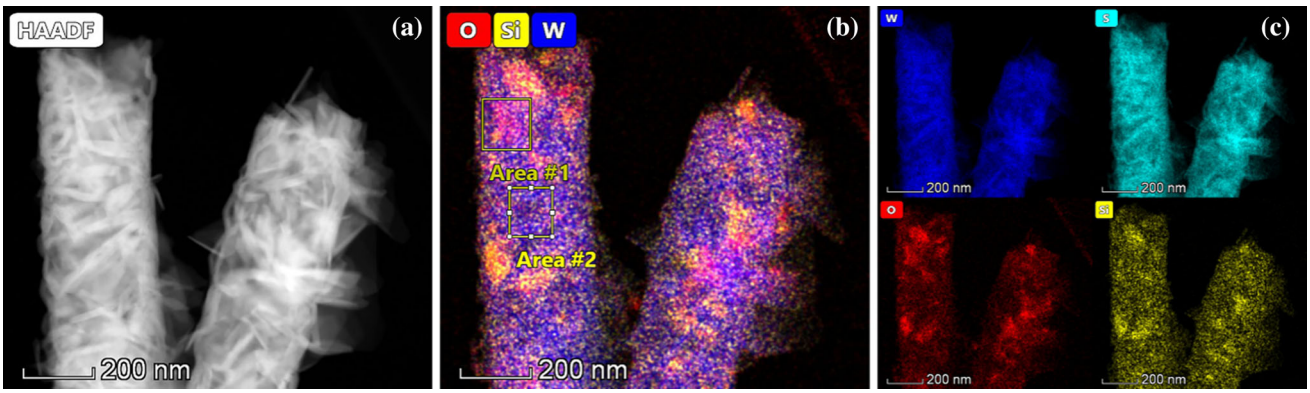

Figure 11 HAADF STEM image of WS_2 fibers (**a**), HAADF STEM EDS elemental maps (**b**, **c**).

Table 4 Quantitative EDS analysis from areas marked in Fig. 11b

Area	Z	Element	Family	Atomic fraction (%)	Atomic error (%)	Mass fraction (%)	Mass error (%)	Fit error (%)
1	8	O	K	9.80	1.66	2.20	0.20	1.95
	14	Si	K	6.31	1.69	2.49	0.56	7.88
	16	S	K	56.95	14.31	25.67	5.31	0.62
	74	W	L	26.94	5.41	69.63	9.85	0.05
2	8	O	K	9.90	1.68	2.23	0.21	2.13
	14	Si	K	6.30	1.69	2.49	0.56	7.88
	16	S	K	56.88	14.29	25.66	5.31	0.62
	74	W	L	26.91	5.41	69.62	9.85	0.05

oxide WO_3 fibers with traces of SiO_2 coming from the $H_4SiW_{12}O_{40}$ precursor and with smaller diameter (335 nm). In the final step, we heated the WO_3 fibers under flow of $H_2/H_2S/N_2$ and converted them to tungsten disulfide WS_2 fibers (av. diam. 196 nm). Based on that experience, we can presume that silicotungstic acid could be a fruitful candidate for water-based scaled up electrospinning followed by after treatment toward WO_3-based materials and other structures.

Acknowledgements

We thank Dr. Y. Feldman for the XRD analysis. This research has been financially supported by the MEYS

CR under the project CEITEC 2020 (LQ1601) and the Horizon 2020 Research and Innovation Programme under the Grant Agreement No. 810626 (SINNCE). CIISB research infrastructure project LM2018127 funded by the MEYS CR is gratefully acknowledged for the financial support of the measurements at the CEITEC MU CF X-ray Diffraction and Bio-SAXS and the CF Cryo-electron Microscopy and Tomography. The support of the Irving and Cherna Moskowitz Center for Nano and Bio-Nano Imaging, the Perlman Family Foundation, the Kimmel Center for Nanoscale Science Grant No. 43535000350000, is greatly acknowledged.

Declartions

Conflict of interest The authors declare no conflicting financial interest.

Supplementary information: The online version contains supplementary material available at https://doi.org/10.1007/s10853-021-05979-y.

References

[1] Ramakrishna S, Fujihara K, Teo W-E, Lim T-C, Ma Z (2005) An introduction to electrospinning and nanofibers. World Sci. https://doi.org/10.1142/5894

[2] Li D, Xia Y (2004) Electrospinning of nanofibers: reinventing the wheel? Adv Mater 16:1151–1170. https://doi.org/10.1002/adma.200400719

[3] Greiner A, Wendorff JH (2007) Electrospinning: a fascinating method for the preparation of ultrathin fibers. Angew Chem Int Ed 46:5670–5703. https://doi.org/10.1002/anie.200604646

[4] Dai Y, Liu W, Formo E, Sun Y, Xia Y (2011) Ceramic nanofibers fabricated by electrospinning and their applications in catalysis, environmental science, and energy technology. Polym Adv Technol 22:326–338. https://doi.org/10.1002/pat.1839

[5] Wu H, Pan W, Lin D, Li H (2012) Electrospinning of ceramic nanofibers: fabrication, assembly and applications. J Adv Ceram 1:2–23. https://doi.org/10.1007/s40145-012-0002-4

[6] Esfahani H, Jose R, Ramakrishna S (2017) Electrospun ceramic nanofiber mats today: synthesis, properties, and applications. Materials 10:1238. https://doi.org/10.3390/ma10111238

[7] Zhou X, Shang C, Gu L, Dong S, Chen X, Han P, Li L, Yao J, Liu Z, Xu H, Zhu Y, Cui G (2011) Mesoporous coaxial titanium nitride-vanadium nitride fibers of core–shell structures for high-performance supercapacitors. ACS Appl Mater Interfaces 3:3058–3063. https://doi.org/10.1021/am200564b

[8] Zhou X, Qiu Y, Yu J, Yin J, Gao S (2011) Tungsten carbide nanofibers prepared by electrospinning with high electrocatalytic activity for oxygen reduction. Int J Hydrogen Energy 36:7398–7404. https://doi.org/10.1016/j.ijhydene.2011.03.081

[9] Yang Y, Wang H, Lu X, Zhao Y, Li X, Wang C (2007) Electrospinning of carbon/CdS coaxial nanofibers with photoluminescence and conductive properties. Mater Sci Eng B 140:48–52. https://doi.org/10.1016/j.mseb.2007.03.010

[10] Jirsak O, Sanetrnik O, Lukas D, Kotek V, Martinova L, Chaloupek J (2005) A Method of nanofibres production from a polymer solution using electrostatic spinning and a device for carrying out the method. WO 2005/024101 A1, 2005

[11] Jirsak O, Petrik S (2012) Recent advances in nanofibre technology: needleless electrospinning. Int J Nanotechnol 9:836–845. https://doi.org/10.1504/IJNT.2012.046756

[12] Zukalova M, Prochazka J, Bastl Z, Duchoslav J, Rubacek L, Havlicek D, Kavan L (2010) Facile conversion of electrospun Tio_2 into titanium nitride/oxynitride fibers. Chem Mater 22:4045–4055. https://doi.org/10.1021/cm100877h

[13] Misono M (2009) Recent progress in the practical applications of heteropolyacid and perovskite catalysts: catalytic technology for the sustainable society. Catal Today 144:285–291. https://doi.org/10.1016/j.cattod.2008.10.054

[14] Kourasi M, Wills RGA, Shah AA, Walsh FC (2014) Heteropolyacids for fuel cell applications. Electrochim Acta 127:454–466. https://doi.org/10.1016/j.electacta.2014.02.006

[15] Mohl M, Rautio A-R, Asres GA, Wasala M, Patil PD, Talapatra S, Kordas K (2020) 2D Tungsten chalcogenides: synthesis, properties and applications. advanced materials. Interfaces 7:2000002. https://doi.org/10.1002/admi.202000002

[16] Eftekhari A (2017) Tungsten dichalcogenides (WS_2, WSe_2, and WTe_2): materials chemistry and applications. J Mater Chem A 5:18299–18325. https://doi.org/10.1039/c7ta04268j

[17] Voiry D, Yamaguchi H, Li J, Silva R, Alves DCB, Fujita T, Chen M, Asefa T, Shenoy VB, Eda E, Chhowalla M (2013) Enhanced catalytic activity in strained chemically exfoliated WS_2 nanosheets for hydrogen evolution. Nat Mater 12:850–855. https://doi.org/10.1038/NMAT3700

[18] Wang K, Feng W-L, Qin X, Deng D-S, Feng X, Zhang C (2017) Tungsten sulfide nanoflakes: synthesis by electrospinning and their gas sensing properties. Z Naturforschung 72(4):375–381. https://doi.org/10.1515/zna-2016-0379

[19] Youn D-H, Kim B-J, Yun SJ (2020) Synthesis and gas sensing properties of WS_2 nanocrystallites assembled hierarchical WS_2 fibers by electrospinning. Nanotechnology 31:105602. https://doi.org/10.1088/1361-6528/ab58a9

[20] Rapoport L, Fleischer N, Tenne R (2005) Applications of WS_2 (MoS_2) inorganic nanotubes and fullerene-like nanoparticles for solid lubrication and for structural nanocomposites. J Mater Chem 15:1782–1788. https://doi.org/10.1039/b417488g

[21] Xu X, Li X, Zhang J, Qiao K, Han D, Wei S, Xing W, Yan Z (2019) Surfactant assisted electrospinning of WS_2 nanofibers and its promising performance as anode material of sodium-ion batteries. Electrochim Acta 302:259–269. https://doi.org/10.1016/j.electacta.2019.02.042

[22] Tenne R, Redlich M (2010) Recent progress in the research of inorganic fullerene-like nanoparticles and inorganic nanotubes. Chem Soc Rev 39:1423–1434. https://doi.org/10.1039/b901466g

[23] Višić B, Panchakarla LS, Tenne R (2017) Inorganic nanotubes and fullerene-like nanoparticles at the crossroads between solid-state chemistry and nanotechnology. J Am Chem Soc 139:12865–12878. https://doi.org/10.1021/jacs.7b01652

[24] Albu-Yaron A, Sinha SS, Tenne R (2020) Nanotubes from two-dimensional materials in contemporary energy research: historical and perspective outlook. ACS Energy Lett 5:1498–1511. https://doi.org/10.1021/acsenergylett.0c00185

[25] Yin W, Liu X, Zhang X, Gao X, Colvin VL, Zhang Y, Yu WW (2020) Synthesis of tungsten disulfide and molybdenum disulfide quantum dots and their applications. Chem Mater 32:4409–4424. https://doi.org/10.1021/acs.chemmater.0c01441

[26] Zhu Y, Zhang X, Ji Y, Feng Y, Zhang J (2013) Fabrication of WS_2 nanofibers from WO_3 nanofibers prepared by an electrospinning method. J Nanosci Nanotechnol 13:1983–1987. https://doi.org/10.1166/jnn.2013.7139

[27] Feldman Y, Frey GL, Homyonfer M, Lyakhovitskaya V, Margulis L, Cohen H, Hodes G, Hutchison JL, Tenne R (1996) Bulk synthesis of inorganic fullerene-like MS_2 (M=Mo, W) from the respective trioxides and the reaction mechanism. J Am Chem Soc 118:5362–5367. https://doi.org/10.1021/ja9602408

[28] Petras D, Mares L, Stranska D (2008) Method and device for production of nanofibers from polymeric solution through electrostatic spinning. US Patent US 2008/0307766A1

[29] Koski A, Yim K, Shivkumar S (2004) Effect of molecular weight on fibrous PVA produced by electrospinning. Mater Lett 58:493–497. https://doi.org/10.1016/S0167-577X(03)00532-9

[30] Tao J, Shivkumar S (2007) Molecular weight dependent structural regimes during the electrospinning of PVA. Mater Lett 61:2325–2328. https://doi.org/10.1016/j.matlet.2006.09.004

[31] Alcohol MP, Clariant (1999)

[32] Pallas NR, Harrison Y (1990) An automated drop shape apparatus and the surface tension of pure water. Colloids Surf 43:169–194. https://doi.org/10.1016/0166-6622(90)80287-E

[33] Zhang C, Yuan X, Wu L, Han Y, Sheng J (2005) Study on morphology of electrospun poly(vinyl alcohol) mats. Eur Polymer J 41:423–432. https://doi.org/10.1016/j.eurpolymj.2004.10.027

[34] Ketpang K, Kim M, Kim S, Shanmugam S (2013) High performance catalyst for electrochemical hydrogen evolution reaction based on SiO_2/WO_{3-x} nanofacets. Int J Hydrog Energy 38:9732–9740. https://doi.org/10.1016/j.ijhydene.2013.05.112

[35] Vasu K, Meiron OE, Enyashin AN, Bar-Ziv R, Bar-Sadan M (2019) Effect of ru doping on the properties of $MoSe_2$ nanoflowers. J Phys Chem C 123:1987–1994. https://doi.org/10.1021/acs.jpcc.8b11712